Supporting Information for

The Linker between the Dimerization and Catalytic Domains of the CheA Histidine Kinase Propagates Changes in Structure and Dynamics Important for the Enzymatic Activity

Xiqing Wang[†], Pramodh Vallurupalli[‡], Anh Vu[†], Kwangwoon Lee[†], Sheng Sun[†], Wen-Ju Bai[†], Chun Wu[†], Hongjun Zhou[†], Joan-Emma Shea[†], Lewis E. Kay[‡], and Frederick W. Dahlquist[†,*]

[†] Department of Chemistry and Biochemistry, University of California Santa Barbara, Santa Barbara, California 93106-9510, USA

[‡] Departments of Molecular Genetics, Biochemistry and Chemistry, University of Toronto, Toronto, Ontario, M5S 1A8, Canada

[*] To whom correspondence should be addressed. Email: dahlquist@chem.ucsb.edu

Figure S1. Domains of CheA. The cartoon structure of monomeric full-length CheA is reconstructed with the structures of *T. maritima* P1 domain (PDB ID: 2LD6), P2 domain in complex with CheY (PDB ID: 1U0S), and the P3P4P5 construct (PDB ID: 1B3Q). Two dashed lines represent the unstructured linkers between the P1 and P2 domains and between the P2 and P3 domains. The P3-P4 and P4-P5 linkers are in red and ATP lid of the P4 domain is colored in light grey.

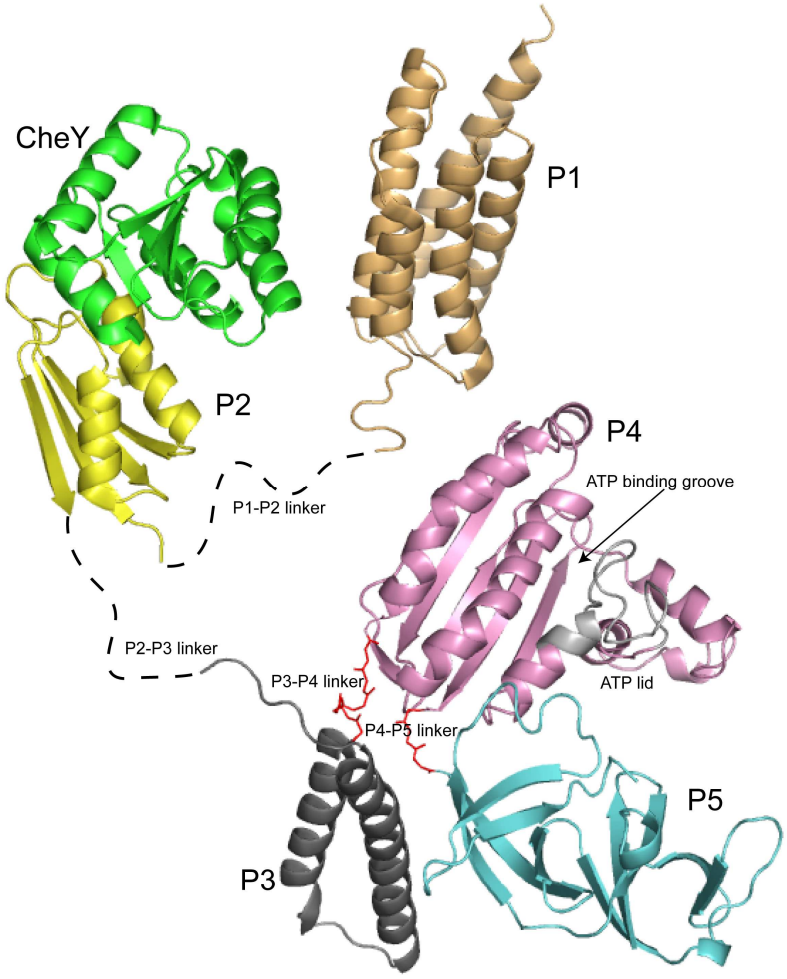

Figure S2. Structural model of chemotaxis signaling complex based on the crystal structures of the CheA dimer (PDB ID: 1B3Q), the CheA–CheW binary complex (PDB ID: 2CH4), and the P4P5–CheW–receptor ternary complex (PDB ID: 3UR1) as well as the EM studies[1,2].

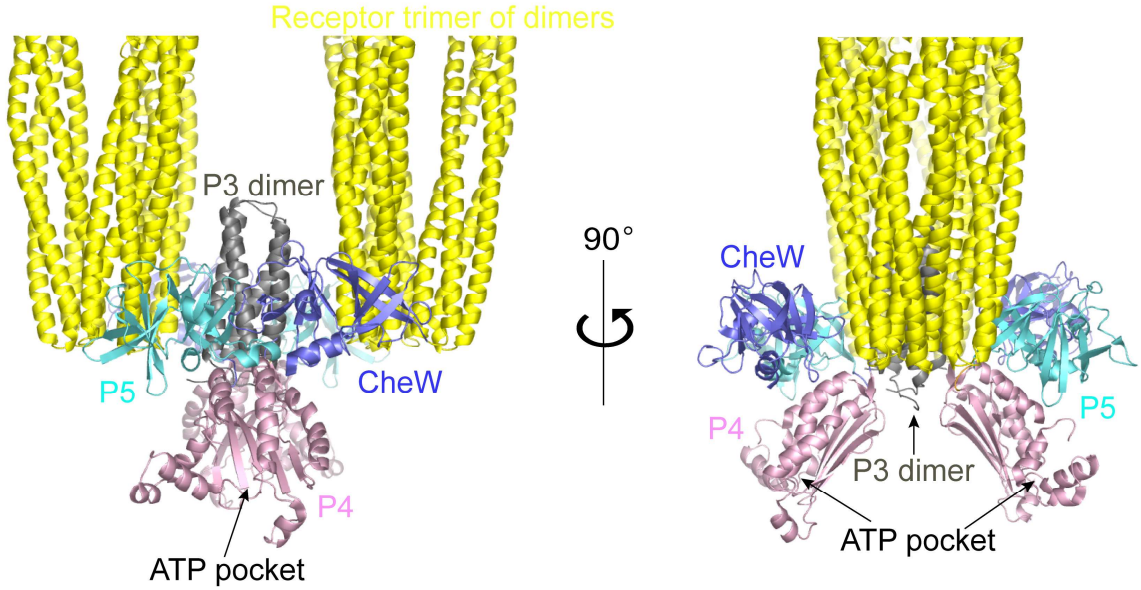

Figure S3. Overlay of the $^{1}H–^{15}N$ TROSY-HSQC spectra of P4 (black) and $P4_l$ (red) labeled with assignments. Resonances showing significant chemical shift changes upon the addition of the linker are in a larger font. Asterisks indicate aliasing of the peak from outside the spectral window along the ^{15}N dimension.

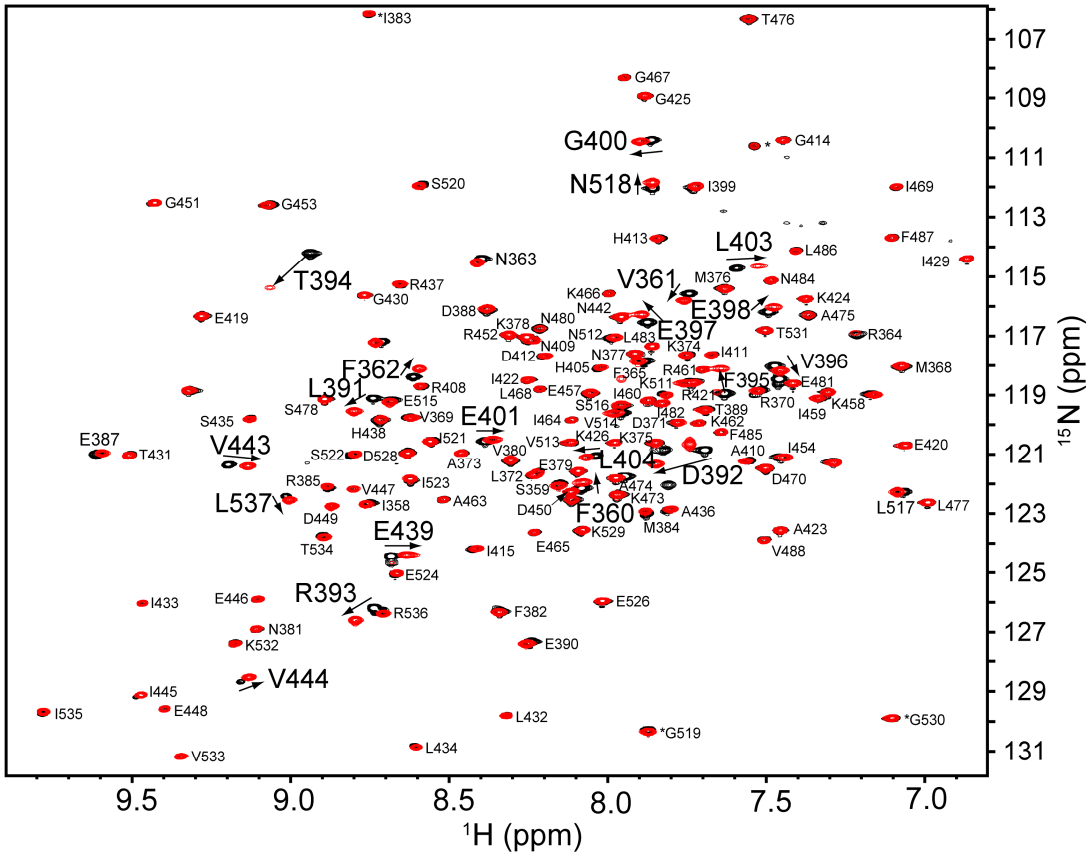

Figure S4. Structural alignment (rmsd=0.99 Å) of the P3P4P5 construct (grey, P5 is omitted) against the backbone atoms of the isolated P4 domain (pink). Except for those at the P4-linker interfaces (Residues 392–394), the residues in the middle helix of the P4 domain do not show significant difference in their X-ray structures. The ATP lid contributes the majority of the rmsd.

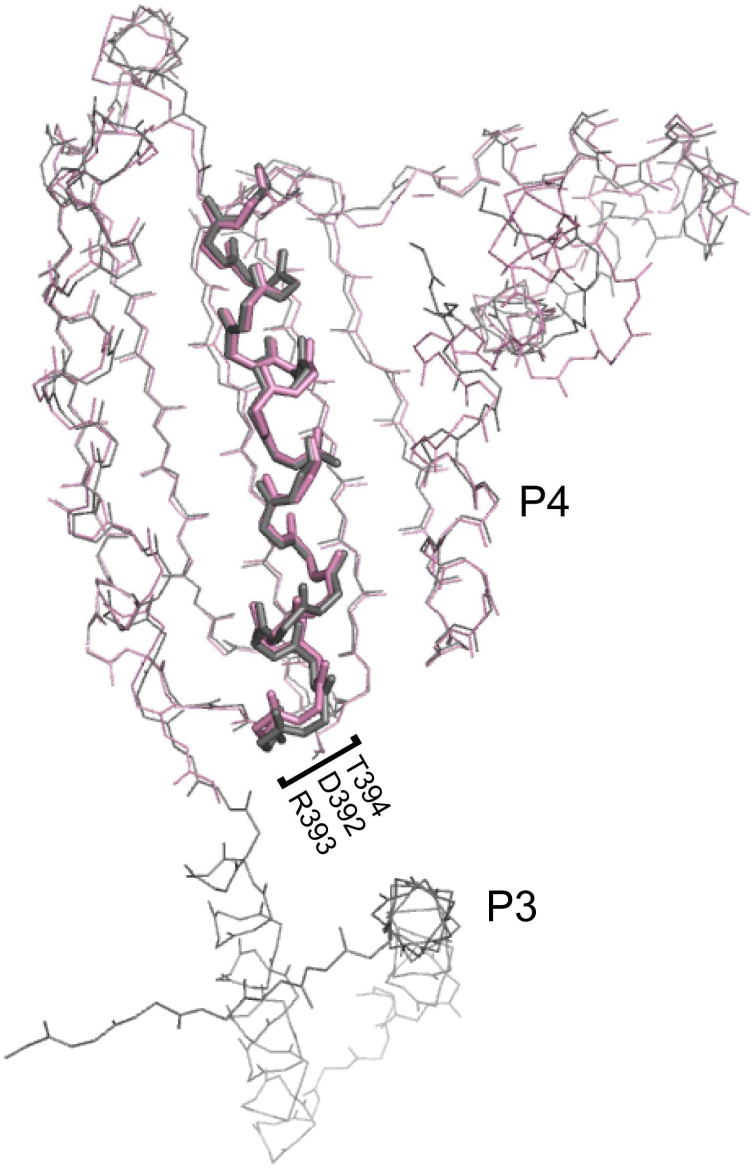

Figure S5. Relaxation dispersion curves show that there is millisecond timescale conformational exchange in $P4_I$. ^{15}N CPMG data for the amide protons (H) and nitrogens (N) of the corresponding residues are shown. Data recorded at 500 and 800 MHz are shown as red and blue dots respectively and the solid lines are the best fits to a global two state process.

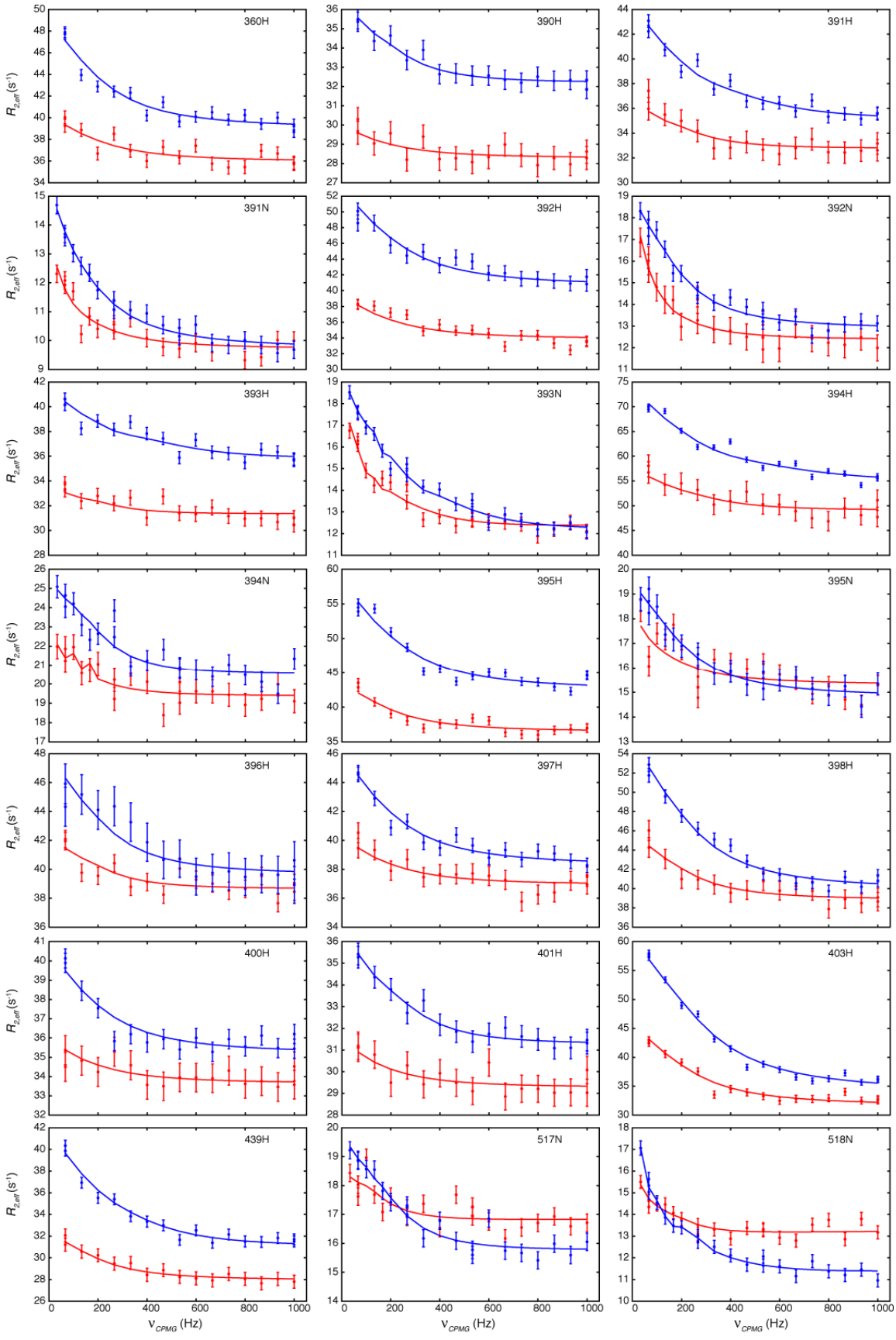
360H
390H
391H
391N
392H
392N
393H
393N
394H
394N
395H
395N
396H
397H
398H
400H
401H
403H
439H
517N
518N
$R_{2,eff}$ (s^{-1})
ν_{CPMG} (Hz)

Figure S6. The exchange contribution to transverse relaxation ($R_{ex} = R_{2,eff}(\nu_{CPMG} = x) - R_{2,eff}(\nu_{CPMG} = 1000$ Hz) , where x = 33 or 66 Hz for ^{15}N and ^{1}H) is plotted with values for P4 with and without the linker indicated along the X- and Y-axis, respectively. Only residues where $R_{ex} > 3$ s^{-1} (800 MHz) in the P4$_l$ construct are included in the comparison.

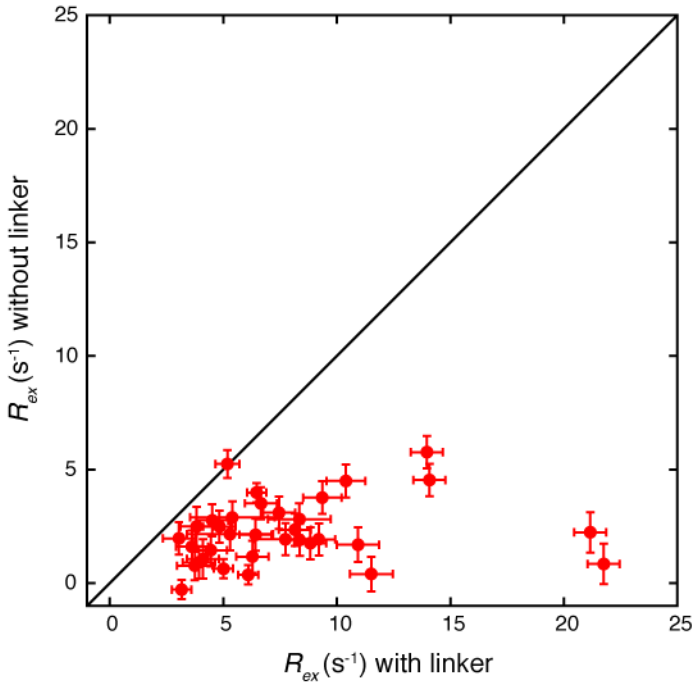

Figure S7. ^{1}H CPMG dispersion profiles recorded at 800 MHz with (red) and without (blue) the P3-P4 linker for two representative residues (394 and 403) showing significant decreases in the sizes of the R_{ex} values when the linker is removed.

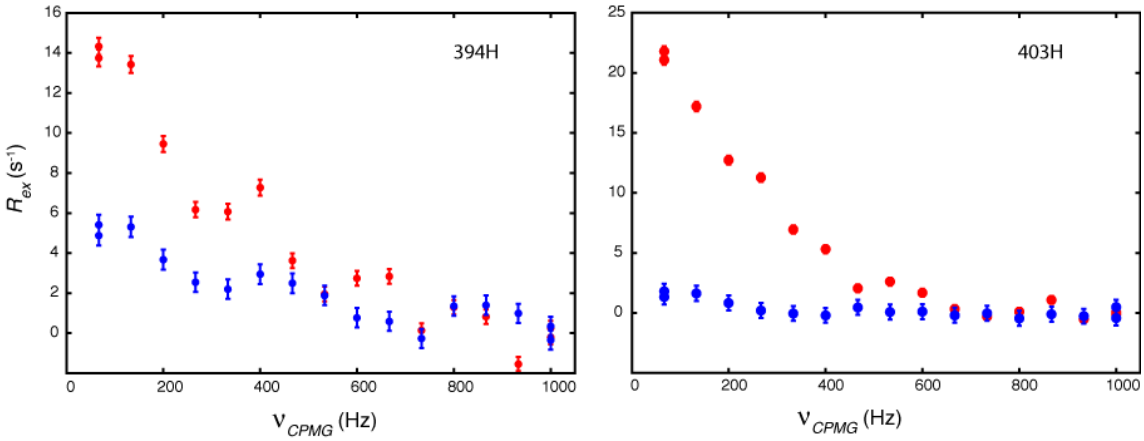

Figure S8. Overlay of the $^{1}H–^{15}N$ TROSY-HSQC spectra of P3P4 (black) and P3P4 R354D (red). Resonances from the P4 domain that disappear or become severely broad are numbered. Some unassigned P3 peaks are identified by superimposing the spectra of the isolated P3 fragment and the P3P4 construct. The assignments of the P4 resonances can be found in Ref. 3 of the SI.

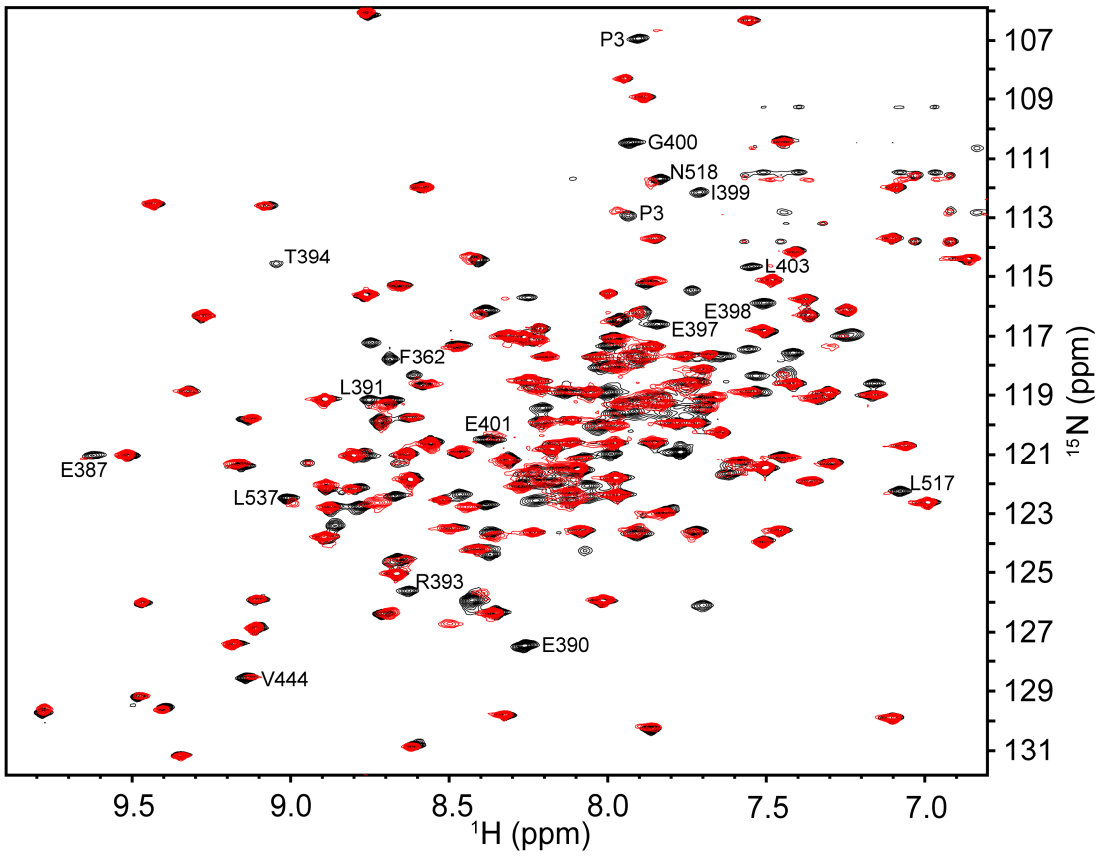

Figure S9. Different conformations of the R354–D392 pair in the crystal structure of the dimeric P3P4P5 (P5 is omitted). A dash line shows the distance between the nitrogen atom (NH2) of Arg354 side chain and the oxygen atom (OD1) of Asp392 side chain.

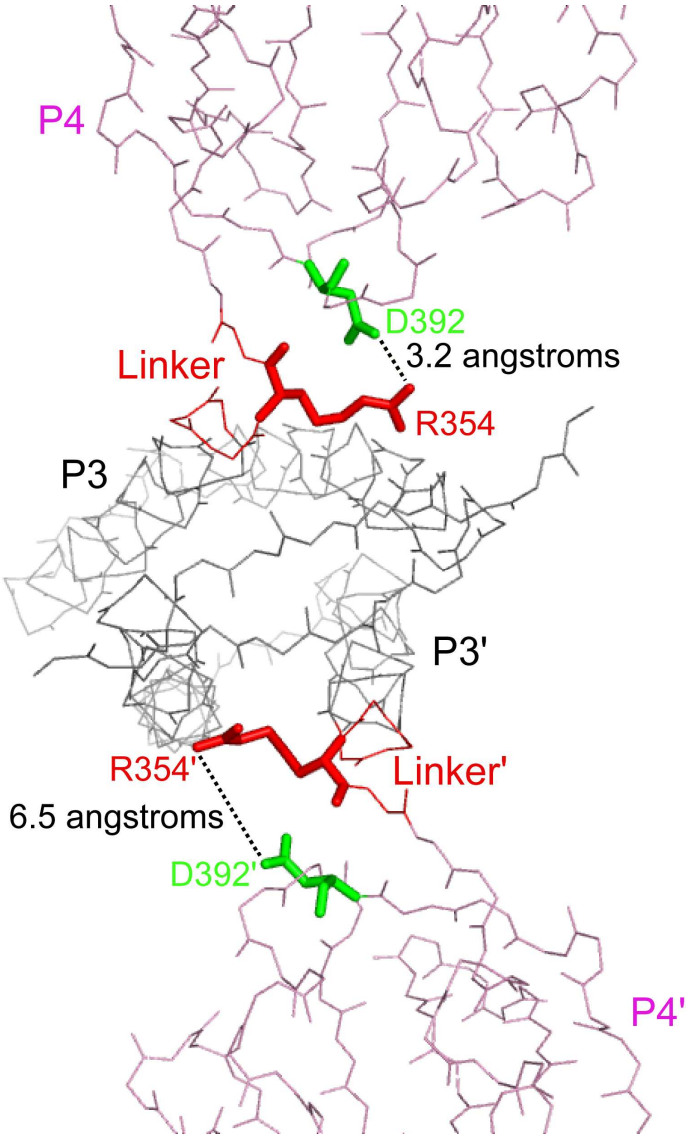

Figure S10. The Arg354–Asp392 pair exists in all the five clusters of the simulation structures (Ref. 4; P5 is omitted). A dash line shows the distance between the nitrogen atom (NH2) of Arg354 side chain and the oxygen atom (OD1) of Asp392 side chain.

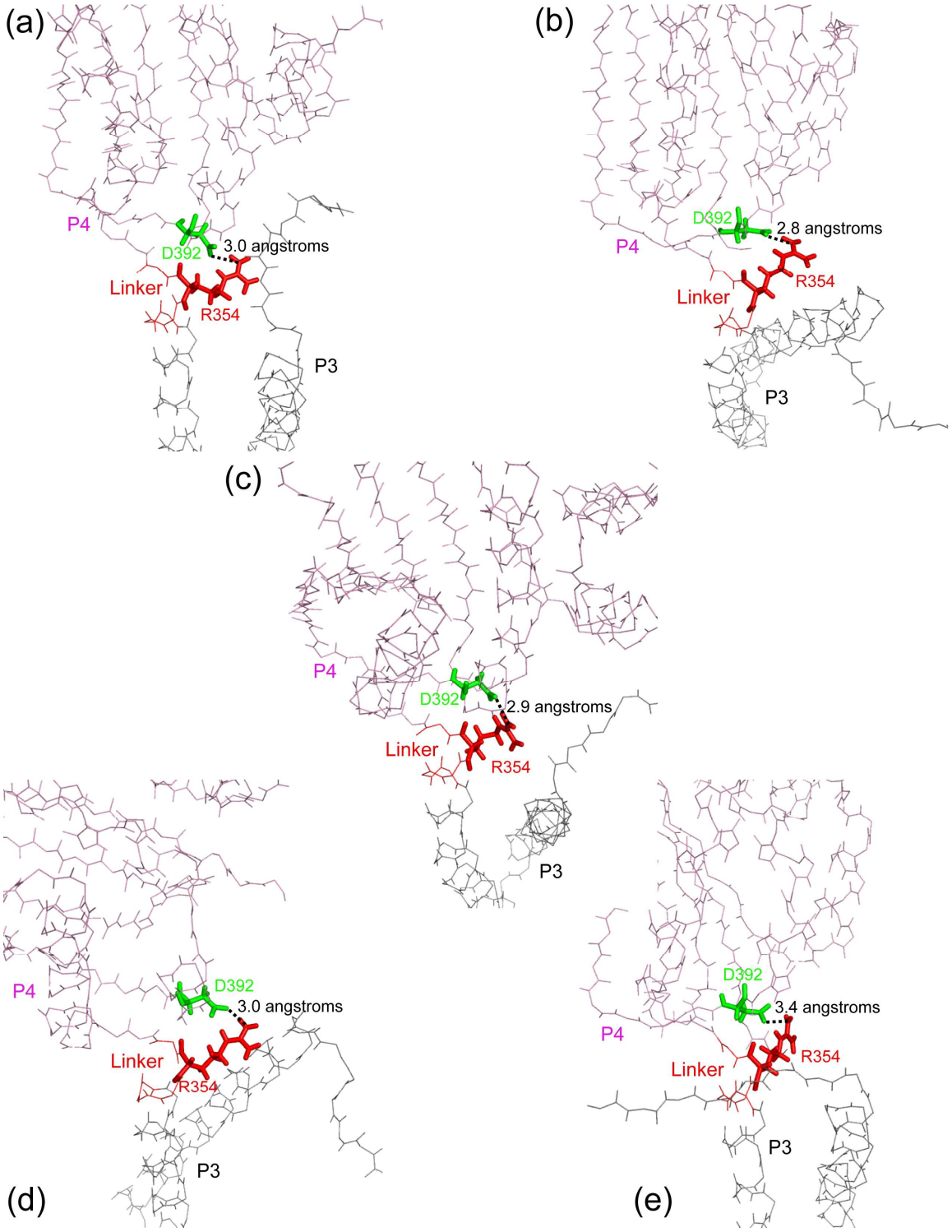
(a)
P4
D392
3.0 angstroms
Linker
R354
P3
(b)
D392
2.8 angstroms
P4
R354
Linker
P3
(c)
P4
D392
2.9 angstroms
Linker
R354
P3
P4
D392
3.0 angstroms
Linker
R354
P3
(d)
D392
3.4 angstroms
P4
R354
Linker
P3
(e)

Figure S11. A representative region of $^{1}H–^{15}N$ TROSY-HSQC spectra of P3P4 (black) and P3P4 M355A. The asterisk indicates aliasing of the peak from outside the spectral window along the ^{15}N dimension.

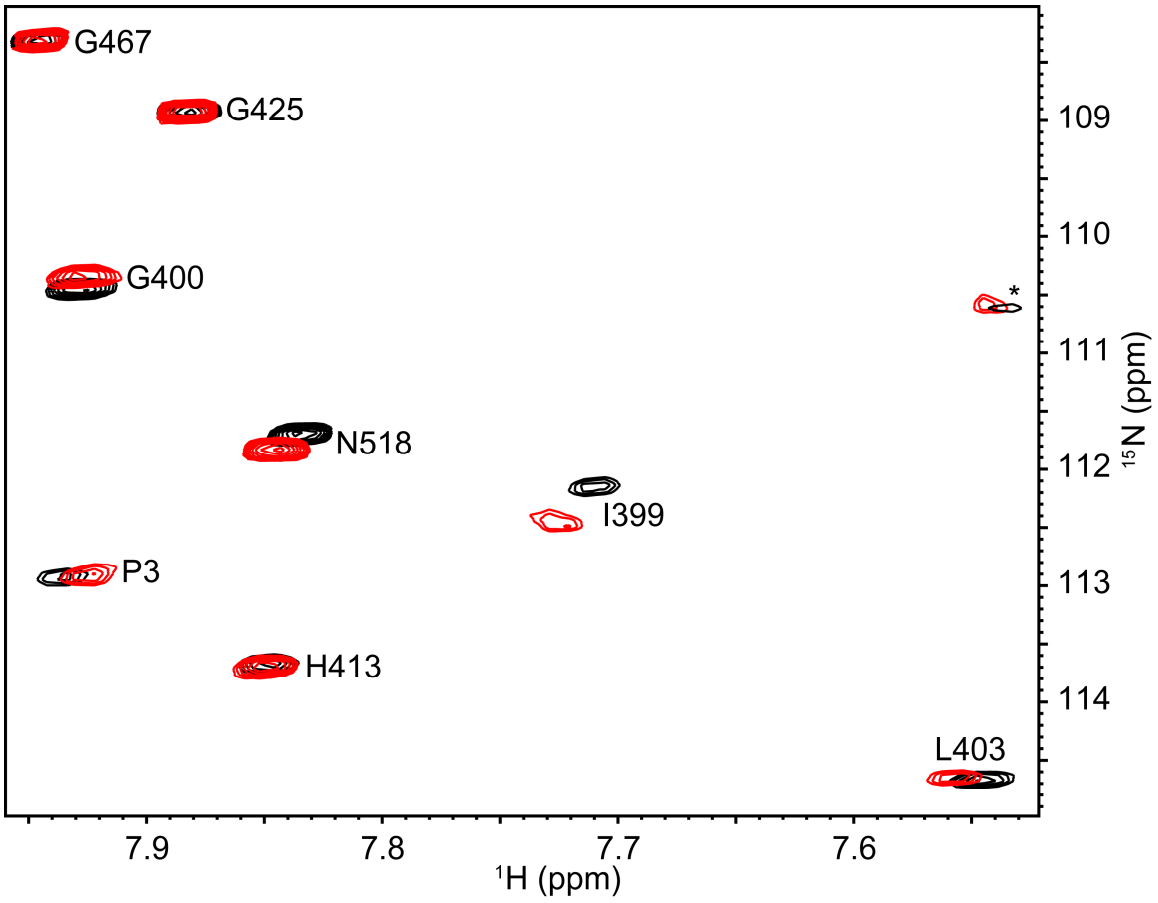

Table S1. Dissociation constants K_d (μM) of CheA variants for TNP-ATP

CheA variant	K_{d1}	K_{d2}
wild type	0.6±0.2	2.4±0.8
K364D	0.9±0.1	3.6±0.4
E368R	0.7±0.2	2.8±0.8
D372R	0.7±0.2	2.8±0.8

References

(1) Briegel, A., Li, X., Bilwes, A. M., Hughes, K. T., Jensen, G. J., and Crane, B.R. (2012). Bacterial chemoreceptor arrays are hexagonally packed trimers of receptor dimers networked by rings of kinase and coupling proteins. *Proc. Natl. Acad. Sci. U. S. A. 109*, 3766–3771.

(2) Liu, J., Hu, B., Morado, D. R., Jani, S., Manson, M. D., and Margolin, W. (2012) Molecular architecture of chemoreceptor arrays revealed by cryoelectron tomography of *Escherichia coli* minicells. *Proc. Natl. Acad. Sci. U. S. A. 109*, E1481–1488.

(3) Hamel, D. J., Zhou, H., Starich, M. R., Byrd, R. A., and Dahlquist, F. W. (2006) Chemical-shift-perturbation mapping of the phosphotransfer and catalytic domain interaction in the histidine autokinase CheA from *Thermotoga maritima*. *Biochemistry 45*, 9509–9517.

(4) Wang, X., Wu, C., Vu, A., Shea, J.–E., and Dahlquist, F. W (2012). Computational and experimental analyses reveal the essential roles of interdomain linkers in the biological function of chemotaxis histidine kinase CheA. *J. Am. Chem. Soc. 134*, 16107–16110.